

In situ synchrotron HE-XRD was used to characterize the deformation and phase transformation evolutions of the Nb nanowires and the NiTi matrix, during the pretreatment (Fig. 4A, inset) and the subsequent tensile cycle (Fig. 4C, inset). After the pretreatment, the Nb nanowires sustained an elastic compressive strain of -1.4% (point D), whereas the NiTi matrix sustained an elastic tensile strain of 1% (point E) (Fig. 4A). There is also some retained B19' phase in the matrix (Fig. 4B). These results can be understood as follows. Upon removal of the pretreatment load, the plastically deformed Nb nanowires (A to B in Fig. 4A) hindered the recovery of the NiTi matrix because of the B19'→B2 transformation (15, 16), which caused large residual strains in the nanowires and the SMA with some retained B19' phase. This demonstrates that strong coupling between the nanowires and the matrix took place during the pretreatment. In the subsequent tensile cycle (Fig. 4C), the elastic strain achieved in the Nb nanowires was up to 5.6% (A to B), consisting of the preexisting elastic compressive strain of -1.4% (O to B) and an elastic tensile strain of 4.2% (O to A). The NiTi matrix went through continuous SIMT throughout the tensile loading and exhibited an ultralow tangential effective modulus (Fig. 4, D and E) rather than undergoing an initial elastic deformation followed by an abrupt SIMT transition, as would occur in a monolithic SMA (16). The continuous SIMT can be ascribed to the contri-

bution of the preexisting internal tensile stress and the retained B19' phase in the matrix. Upon unloading, the NiTi matrix underwent a reverse transformation from the stress-induced martensite to the parent phase (Fig. 4, D and E), introducing a small hysteresis in the stress-strain curve resulting from energy dissipation during the process. The experimental evidence presented above demonstrates that the Nb nanowires experienced an ultrawide elastic strain of $4.2\% - (-1.4\%) = 5.6\%$, which closely matches the phase transformation strain of $\sim 7\%$ of NiTi. This matching of elastic and transformation strains results in the extraordinary properties of NICSMA.

References and Notes

1. M. F. Ashby, *Materials Selection in Mechanical Design* (Butterworth-Heinemann, Burlington, VT, 2005).
2. T. Saito *et al.*, *Science* **300**, 464 (2003).
3. E. W. Wong, P. E. Sheehan, C. M. Lieber, *Science* **277**, 1971 (1997).
4. T. Zhu, J. Li, *Prog. Mater. Sci.* **55**, 710 (2010).
5. Y. Yue, P. Liu, Z. Zhang, X. Han, E. Ma, *Nano Lett.* **11**, 3151 (2011).
6. G. Richter *et al.*, *Nano Lett.* **9**, 3048 (2009).
7. L. Tian *et al.*, *Nat Commun.* **3**, 609 (2012).
8. K. Koziol *et al.*, *Science* **318**, 1892 (2007).
9. D. A. Walters *et al.*, *Appl. Phys. Lett.* **74**, 3803 (1999).
10. Y. Dzenis, *Science* **319**, 419 (2008).
11. P. Podsiadlo *et al.*, *Science* **318**, 80 (2007).
12. J. N. Coleman, U. Khan, Y. K. Gun'ko, *Adv. Mater.* **18**, 689 (2006).
13. L. Thilly *et al.*, *Acta Mater.* **57**, 3157 (2009).
14. V. Vidal *et al.*, *Scr. Mater.* **60**, 171 (2009).
15. K. Otsuka, C. M. Wayman, Eds., *Shape Memory Materials* (Cambridge Univ. Press, Cambridge, 1998).

16. K. Otsuka, X. Ren, *Prog. Mater. Sci.* **50**, 511 (2005).
17. S. Ogata, J. Li, S. Yip, *Science* **298**, 807 (2002).
18. M. Piao, S. Miyazaki, K. Otsuka, *Mater. Trans. Jpn. Inst. Met.* **33**, 337 (1992).
19. See supplementary materials on Science Online.
20. C. C. Aydiner, D. W. Brown, N. A. Mara, J. Almer, A. Misra, *Appl. Phys. Lett.* **94**, 031906 (2009).
21. L. Thilly *et al.*, *Appl. Phys. Lett.* **88**, 191906 (2006).
22. C. Scheuerlein, U. Stuhr, L. Thilly, *Appl. Phys. Lett.* **91**, 042503 (2007).
23. M. Niinomi, M. Nakai, *Int. J. Biomater.* **2011**, 1 (2011).
24. M. Niinomi, *Metall. Mater. Trans. A Phys. Metall. Mater. Sci.* **33**, 477 (2002).
25. D. C. Hofmann *et al.*, *Nature* **451**, 1085 (2008).

Acknowledgments: We thank G. H. Wu, H. B. Xu, and Y. F. Zheng for valuable discussions on the deformation mechanism of NICSMA. This work is supported by the key program project of National Natural Science Foundation of China (NSFC) (51231008), the National 973 programs of China (2012CB619400 and 2009CB623700), and the NSFC (51071175, 51001119, 50831001, and 10825419). J.L. also acknowledges support by NSF DMR-1008104 and DMR-1120901. X.D.H. acknowledges support by the Beijing High-level Talents (PHR20100503), the Beijing PXM201101420409000053, and Beijing 211 project. D.E.B. acknowledges support by the Institute for NanoScience, Engineering, and Technology (INSET) of Northern Illinois University. Use of the Advanced Photon Source was supported by the U.S. Department of Energy, Office of Science, under contract no. DE-AC02-06CH11357.

Supplementary Materials

www.sciencemag.org/cgi/content/full/339/6124/1191/DC1
Materials and Methods
Figs. S1 to S12
References (26–30)

9 August 2012; accepted 10 January 2013
10.1126/science.1228602

Terrestrial Accretion Under Oxidizing Conditions

Julien Siebert,^{1*} James Badro,² Daniele Antonangeli,¹ Frederick J. Ryerson^{2,3}

The abundance of siderophile elements in the mantle preserves the signature of core formation. On the basis of partitioning experiments at high pressure (35 to 74 gigapascals) and high temperature (3100 to 4400 kelvin), we demonstrate that depletions of slightly siderophile elements (vanadium and chromium), as well as moderately siderophile elements (nickel and cobalt), can be produced by core formation under more oxidizing conditions than previously proposed. Enhanced solubility of oxygen in the metal perturbs the metal-silicate partitioning of vanadium and chromium, precluding extrapolation of previous results. We propose that Earth accreted from materials as oxidized as ordinary or carbonaceous chondrites. Transfer of oxygen from the mantle to the core provides a mechanism to reduce the initial magma ocean redox state to that of the present-day mantle, reconciling the observed mantle vanadium and chromium concentrations with geophysical constraints on light elements in the core.

The depletion of siderophile (i.e., “iron-loving”) elements in Earth’s mantle relative to chondrites can constrain the redox state of accreting materials during terrestrial accretion and core differentiation (1–4). For example, metal-

silicate partitioning experiments at atmospheric pressure indicate that the observed depletion of slightly siderophile elements (SSEs) such as V and Cr can only be produced at conditions more reducing than those required to account for the abundance of moderately siderophile elements (such as Ni, Co, and W) or highly siderophile elements (5). Using metal-silicate partition coefficients obtained at pressures up to 25 GPa, homogeneous accretion models posit that metal-silicate equilibrium took place at the base of a deep terrestrial magma ocean at a single oxygen fugacity (f_{O_2}) (6–8). However, the pressure-temperature (P - T)

conditions required to produce the observed depletions for V and Cr (at the present-day f_{O_2}) require temperatures that greatly exceed that of the mantle liquidus (2, 4, 9, 10). Such conditions are physically inconsistent with the magma ocean hypothesis, where the P - T conditions at the base of a magma ocean necessarily lie between the mantle solidus and liquidus, thereby creating a rheological boundary that enables the metal to pond and equilibrate with the silicate melt.

To satisfy this rheological constraint and SSE abundance patterns, recent models of core formation constrain metal-silicate equilibration to the P - T conditions of the peridotite liquidus and invoke early accretion of highly reduced materials with a FeO-poor silicate component (2, 4, 10, 11). These initially low f_{O_2} conditions ($\sim 1W-4$, corresponding to 4 log f_{O_2} units below the iron-wüstite buffer) enhance the siderophile character of the SSEs at the relevant P - T conditions. Subsequent, gradual oxidation of the mantle to $\sim 1W-2$ over the course of core formation is required to account for moderately siderophile element abundances and, most important, to reach the current mantle FeO content [8 weight percent (wt %) FeO in silicate]. Under reducing conditions, silicon is likely to be the only light element entering the core in large amounts (10–12). This scenario relies on extensive pressure and temperature extrapolation of SSE partitioning data, as existing results are restricted to rela-

¹Institut de Minéralogie et de Physique des Milieux Condensés, Université Pierre et Marie Curie, UMR CNRS 7590, Institut de Physique du Globe de Paris, 75005 Paris, France. ²Institut de Physique du Globe de Paris, Université Paris Diderot, 75005 Paris, France. ³Lawrence Livermore National Laboratory, Livermore, CA 94551, USA.

*To whom correspondence should be addressed. E-mail: julien.siebert@impmc.upmc.fr

tively low- P , low- T conditions (up to 25 GPa and 3000 K) and do not cover a large fraction of the P - T conditions relevant to core-mantle equilibrium in a deep magma ocean (up to 60 GPa and 4000 K) (13, 14). Should the solubility of additional components, such as oxygen, be enhanced in this P - T range, their influence on the thermodynamics of the metallic phase would not be captured by extrapolation.

Here, we present partitioning data for V and Cr at the conditions directly equivalent to the full range of P - T conditions relevant to core formation and metal-silicate equilibration at the base of a deep magma ocean (Fig. 1). The experiments were performed in a laser-heated diamond anvil cell (LHDAC) (15) between 35 and 74 GPa and between 3100 and 4400 K. We found that the mantle concentration of Cr and V can be satisfied in a single high- P , high- T equilibrium (Fig. 1) in relatively oxidizing conditions. In fact, core formation is a continuous process taking place over the course of accretion, with the core and man-

tle continuously growing and segregating from one another (2, 4). Metal-silicate partition coefficients for SSEs along any possible thermodynamic path (P , T , composition) hypothesized during core formation are required to accurately calculate mantle siderophile trace element concentrations. The P - T conditions of core formation necessarily increase as Earth grows, but there is no robust constraint on the evolution and composition of accretionary material. The composition of these materials does, however, establish the initial oxidation state of Earth's interior—an important variable controlling metal-silicate equilibrium. Hence, siderophile element partitioning provides a diagnostic by which the composition of accretionary materials may be inferred.

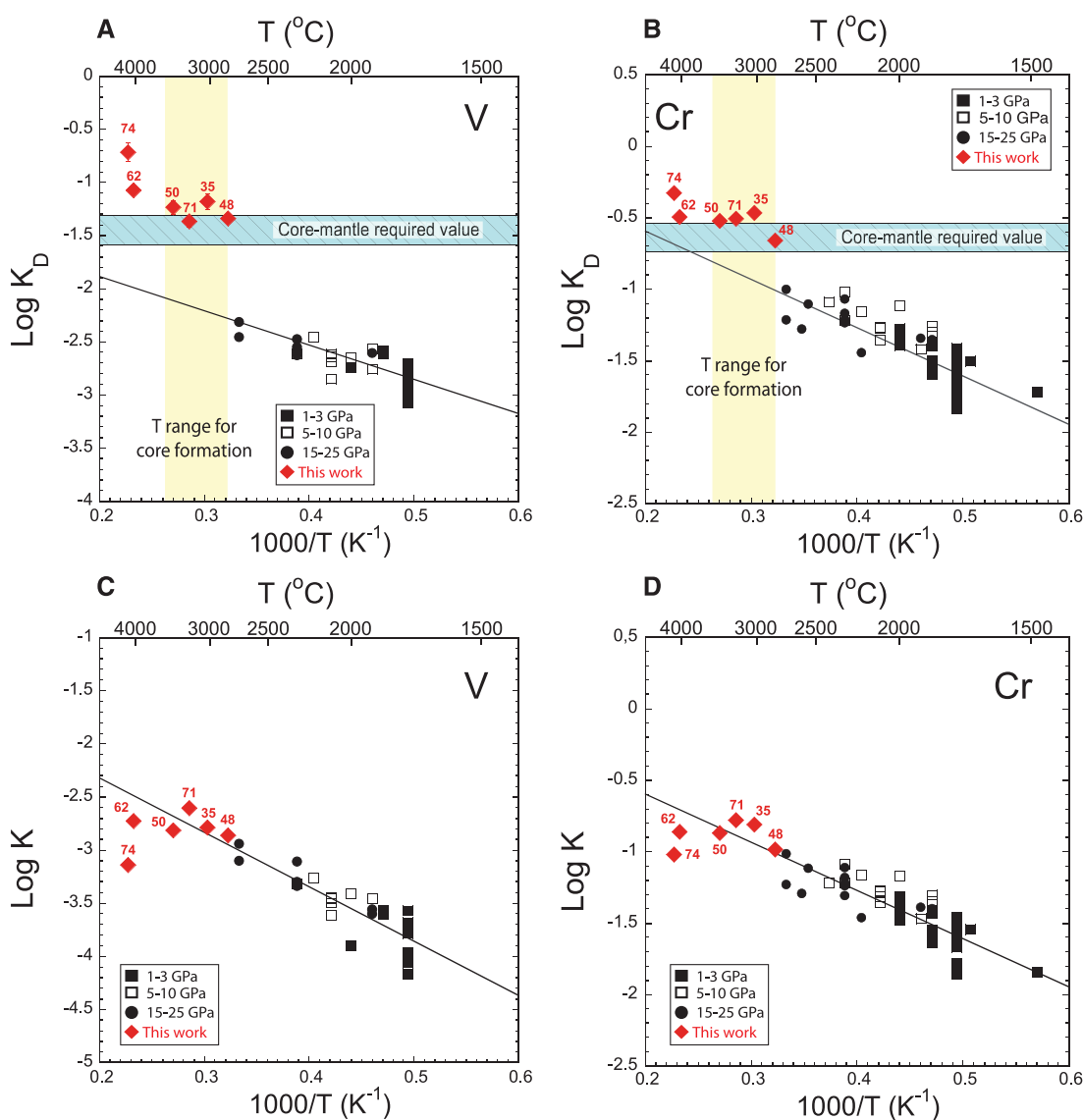
Plausible accretionary composition models coupled with core formation scenarios can be tested against observables to constrain better the nature of the building blocks of Earth. For any core formation model, the primary metrics are (i) that final silicate mantle composition coin-

cides with present-day mantle compositions, and (ii) that the composition of the core is consistent with geophysical observations. In terms of composition, the most important influence on partitioning is fO_2 , which describes the redox state of the accretionary environment and controls the FeO content of the silicate magma ocean. The effect of core formation on the siderophile trace element concentration in the mantle cannot be determined unless the partition coefficient is known as a function of P , T , and fO_2 . The Fe-normalized partition coefficient (K_D) of an element M can be parameterized as

$$\log \frac{D_M}{D_{Fe^{n/2}}} = \log K_D = a + \frac{b}{T} + \frac{c \cdot P}{T} - \log \frac{\gamma_M}{\gamma_{Fe^{n/2}}} \quad (1)$$

where n is the valence of element M , γ_{Fe} and γ_M are the activity coefficients of iron and cation M

Fig. 1. (A and B) Exchange coefficients (K_D) for V (A) and Cr (B) plotted as a function of reciprocal temperature: this work (red diamonds with labeled pressure conditions in GPa) and other studies (2, 9, 10, 16–19) at different pressure conditions. Where no error bars are shown, the uncertainties do not exceed the symbol size. The solid lines are the result of least-squares regressions of previous lower-pressure partitioning data (2, 9, 10, 16–19). The partitioning data from our DAC experiments, well above the low-pressure regression, are attributed to the influence of oxygen solubility in the metal on the activity coefficients of Cr and V in the metal. (C and D) Equilibrium constant K [i.e., K_D corrected for activity coefficients (15), $K = K_D \cdot (\gamma_M/\gamma_{Fe}^{n/2})$] for V (C) and Cr (D) as a function of reciprocal temperature. This is the same data set as in (A) and (B), except that the exchange coefficient has been corrected for the activity coefficients of Fe, Cr, and V. These values depend strongly on oxygen content in the metallic phase. All data (O-bearing and O-depleted) fall on a single linear trend, showing the consistency of our activity model. Note that it is difficult to correct the activity in metals that are too O-rich, like our point at 74 GPa that has the highest O content in the metal (17 wt %), which falls systematically below the trend; however, high oxygen concentration increases the siderophile behavior of V and Cr.



in the metal phase, respectively, and a , b , and c are regression constants.

In accord with results from large-volume press (LVP) experiments at lower pressure (2, 9, 10, 16–19), we see that the K_D values for Cr and V obtained in the LHDAC both increase with temperature between 35 and 74 GPa and are relatively insensitive to pressure (Fig. 1, A and B). However, the results of our experiments show that Cr and V are more siderophile

(higher K_D) than would be expected from the extrapolation of lower- P , lower- T data and directly match the terrestrial target values (Fig. 1, A and B). Indeed, all of our data lie above the trend extrapolated from lower- P , lower- T LVP experiments. This is due to another important parameter that influences metal-silicate partitioning: the presence of minor constituents in the metallic phase, which in turn affects the activity coefficients of the siderophile elements (the last

term in Eq. 1). In the high- P , high- T , high- f_{O_2} (~IW-1) conditions of our experiments (15), large amounts of oxygen (between 3.7 and 17 wt %) are present in the metallic phase (tables S2 and S3). This alters the activities of Cr and V in iron (20, 21) and explains the disparity between our results and those extrapolated from lower- P experiments in which the metallic phases contain negligible oxygen. We used the epsilon formalism (22) to calculate the activity coefficients

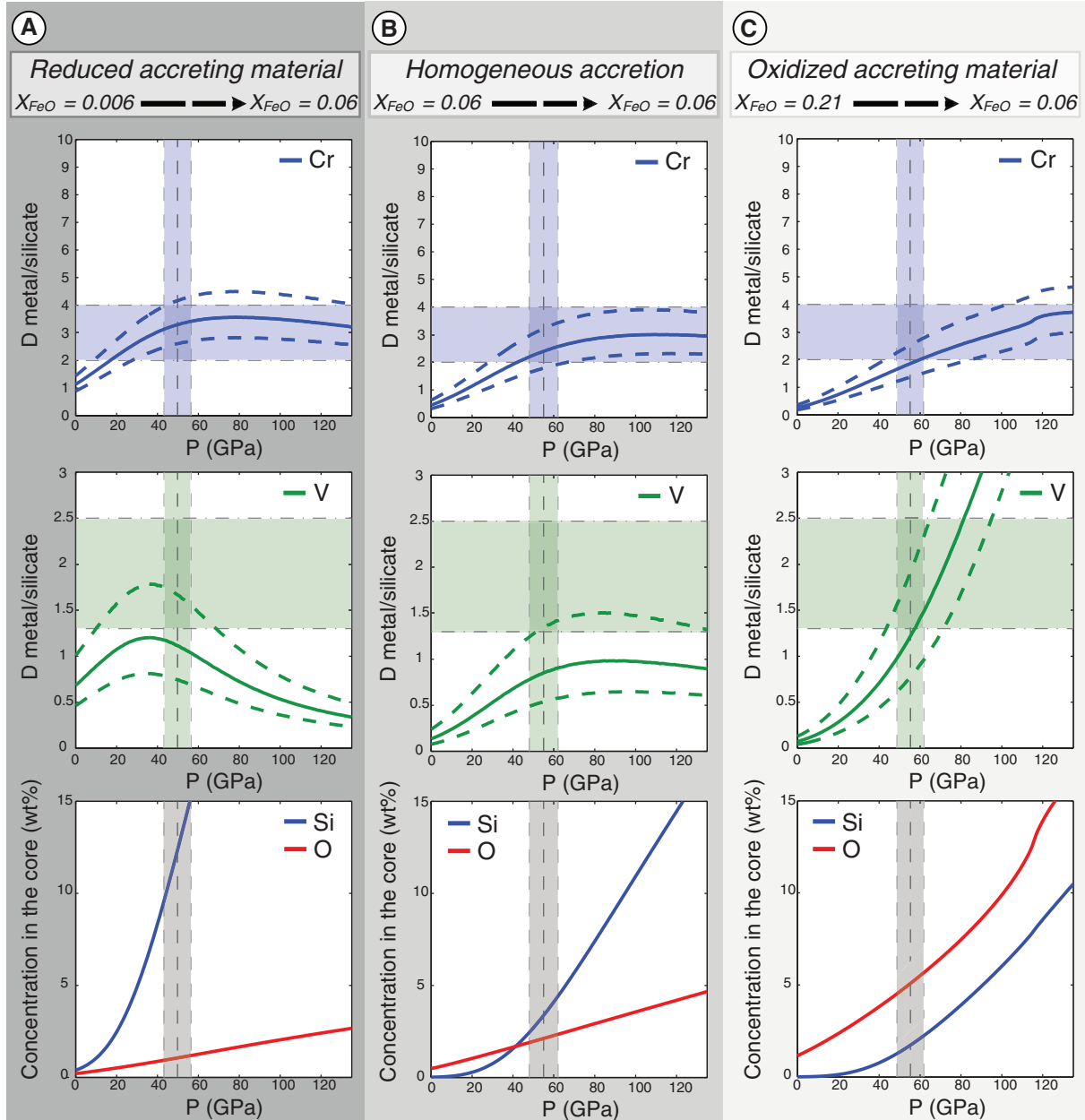


Fig. 2. Final core-mantle partition coefficients of Cr and V (D_{Cr} and D_V , top and middle rows) resulting from continuous core formation, as a function of final magma ocean pressure (i.e., depth). Solid lines show the evolution of the average partition coefficients; dashed lines define the uncertainty envelope calculated by Monte Carlo propagation of all uncertainties listed in table S4. The horizontal shaded bars represent the observed terrestrial target values for Cr and V (9). The bottom row shows the concentrations of O and Si in the core. The calculations are performed along three different oxygen

fugacity paths: (A) the highly reduced model, (B) the homogeneous accretion model, and (C) the oxidized model. The relative size of the magma ocean with respect to that of the whole mantle was varied from a shallow magma ocean (final pressure of 0 GPa) to a global magma ocean (final pressure of 135 GPa). The gray vertical shaded bars show the pressure range where Cr and V abundances match the target values, along with additional constraints from Ni and Co partitioning (15). They show that the core must have formed at a final pressure between 40 and 60 GPa.

for Cr and V due to the incorporation of oxygen, correcting both the LHDAC and lower- P data (2, 9, 10, 16–19) to obtain an equilibrium constant $K = K_D(\gamma_M/\gamma_{Fe}^{n/2})$, where γ_M is the activity coefficient for element M at the relevant oxygen concentration. The low- P and high- P data follow a linear trend (Fig. 1, C and D), supporting our contention that the apparent discrepancy between the low- P and high- P values of K_D (Fig. 1, A and B) is entirely due to the change in activity coefficient resulting from enhanced oxygen solubility in our experiments. The regression constants a , b , and c and activity models using LVP data [for experiments with metal phases containing no additional light elements such as C and S (2, 9, 10, 16–19)] combined with our data are reported in table S4 (15).

We used the results of our regression in a continuous core formation model (2, 4) to evaluate the influence of oxidation state on the core-mantle evolution of SSEs (15). We explored all possible magma ocean depths (from 0 to 100% of the mantle) and all possible geotherms relevant to the base of that magma ocean (temperatures between the mantle solidus and liquidus) (23, 24). Three accretionary models distinguished by the compositions of accretionary components and oxidation/reduction paths during planetary growth were considered: (i) a reduced model (4, 10), in which the initial 28% of accretion is characterized by the addition of highly reduced material (0.6 wt % FeO in the mantle) followed by continuous oxidation to yield a mantle with the current FeO content of 8 wt %; (ii) a homogeneous accretion model, in which the FeO content of the mantle is constant and equal to its present value over the entire course of accretion; and (iii) an oxidized model, in which Earth accretes from oxidized material, such as carbonaceous chondrites or a mixture (21% FeO in the mantle) of chondrites (25), and is then gradually reduced (through O solubility in the core) until the FeO content of the mantle reaches the present-day value.

The partition coefficients D_V and D_{Cr} evolve as a function of magma ocean depth (Fig. 2) for the three accretionary scenarios (fig. S2 reports results for D_{Ni} and D_{Co}). We find that the redox state of the accreting material only slightly influences the acceptable range of magma ocean depths, 50 to 56 (± 7) GPa. In contrast to previous investigations (2, 4, 9–11, 26), we show that the terrestrial SSE partition coefficients (V and Cr) can be satisfied with any of our three accretion models. On the basis of our data, there is no requirement that accretion must have occurred under highly reducing conditions in order to explain present-day mantle siderophile trace element concentrations. This contradicts previous claims (2, 4, 10, 11) that V and Cr constrain the redox conditions of core formation and terrestrial accretion to allow only the highly reduced model.

The f_{O_2} path during terrestrial accretion also strongly affects the concentration of light elements in the core. On the basis of our LHDAC

partitioning experiments, we calculate the O and Si concentrations in the core (table S5) and find that the highly reduced model leads to excessively high concentrations of silicon in the core, above 10 wt %, along with less than 1 wt % oxygen (Fig. 2, bottom row). The constant FeO-homogeneous accretion model leads to a core containing 2.5 to 5.5 wt % Si and 2 to 2.5 wt % O, whereas the oxidized path yields an oxygen-rich core with 4.5 to 5.5 wt % O and 1.5 to 2.2 wt % Si. The Si content of the core in the highly reduced model (>10 wt %) is incompatible with cosmochemical and geophysical constraints. Indeed, cosmochemical models (27–29) suggest that the upper limit for Si content in the core is 8 wt %. High-pressure measurements of sound velocities in iron and iron alloys indicate that the core must contain between 1 and 4 wt % Si for it to be compatible with seismic radially averaged wave speeds and densities (30, 31).

Terrestrial accretion under relatively oxidizing conditions requires a mechanism for reducing the mantle to yield an oxidation state and FeO concentration compatible with present-day conditions. Because our model requires large concentrations of oxygen in the core, transferring FeO from the silicate mantle to the core solves both problems: reducing FeO in the mantle and increasing O in the core, while at the same time rendering the SSEs more siderophile because of the thermodynamic influence of enhanced oxygen solubility on their activities. This mechanism of FeO solubility in the core has been proposed to explain the difference in mantle redox between Earth and Mars (32).

A mutually compatible solution to the problems of light elements in the core and trace siderophile element concentrations in the mantle is a major discriminant in validating various models of accretion and core formation. On this basis, we show that it is unlikely that Earth formed under highly reduced conditions, such as those found in enstatite chondrites. Conversely, accretion under oxidized conditions similar to those of the most common meteorites (e.g., ordinary and/or carbonaceous chondrites) is consistent with the siderophile trace element concentrations in the mantle and with the geophysical constraints on the composition of the core. Finally, accretion of large objects (planetesimals and planetary embryos) that had redox conditions similar ($\sim 1W-2.3$) to those of Earth also satisfies the geochemical and geophysical constraints, while at the same time proving the most realistic in terms of dynamical planetary formation models (33).

References and Notes

- H. S. C. O'Neill, *Geochim. Cosmochim. Acta* **55**, 1159 (1991).
- J. Wade, B. J. Wood, *Earth Planet. Sci. Lett.* **236**, 78 (2005).
- H. Wänke, T. Gold, *Philos. Trans. R. Soc. London Ser. A* **303**, 287 (1981).
- B. J. Wood, M. J. Walter, J. Wade, *Nature* **441**, 825 (2006).

- A. E. Ringwood, *Geochim. Cosmochim. Acta* **30**, 41 (1966).
- K. G. Gessmann, D. C. Rubie, *Earth Planet. Sci. Lett.* **184**, 95 (2000).
- J. Li, C. B. Agee, *Nature* **381**, 686 (1996).
- K. Righter, M. J. Drake, G. Yaxley, *Phys. Earth Planet. Inter.* **100**, 115 (1997).
- J. Siebert, A. Corgne, F. J. Ryerson, *Geochim. Cosmochim. Acta* **75**, 1451 (2011).
- B. J. Wood, J. Wade, M. R. Kilburn, *Geochim. Cosmochim. Acta* **72**, 1415 (2008).
- D. C. Rubie *et al.*, *Earth Planet. Sci. Lett.* **301**, 31 (2011).
- A. Ricolleau, Y. Fei, A. Corgne, J. Siebert, J. Badro, *Earth Planet. Sci. Lett.* **310**, 409 (2011).
- J. Siebert, J. Badro, D. Antonangeli, F. J. Ryerson, *Earth Planet. Sci. Lett.* **321–322**, 189 (2012).
- M. A. Bouhifd, A. P. Jephcoat, *Earth Planet. Sci. Lett.* **307**, 341 (2011).
- See supplementary materials on Science Online.
- N. L. Chabot, C. B. Agee, *Geochim. Cosmochim. Acta* **67**, 2077 (2003).
- C. K. Geßmann, D. C. Rubie, *Geochim. Cosmochim. Acta* **62**, 867 (1998).
- U. Mann, D. J. Frost, D. C. Rubie, *Geochim. Cosmochim. Acta* **73**, 7360 (2009).
- J. Wade, B. J. Wood, *Nature* **409**, 75 (2001).
- A. Corgne, J. Siebert, J. Badro, *Earth Planet. Sci. Lett.* **288**, 108 (2009).
- A. E. Ringwood, T. Kato, W. Hibberson, N. Ware, *Nature* **347**, 174 (1990).
- Z. Ma, *Mater. Mater. Trans. B* **32**, 87 (2001).
- D. Andraut *et al.*, *Earth Planet. Sci. Lett.* **304**, 251 (2011).
- G. Fiquet *et al.*, *Science* **329**, 1516 (2010).
- C. Fitoussi, B. Bourdon, *Science* **335**, 1477 (2012).
- A. Corgne, S. Keshav, B. J. Wood, W. F. McDonough, Y. Fei, *Geochim. Cosmochim. Acta* **72**, 574 (2008).
- C. J. Allegre, J. P. Poirier, E. Humler, A. W. Hofmann, *Earth Planet. Sci. Lett.* **134**, 515 (1995).
- M. Javoy *et al.*, *Earth Planet. Sci. Lett.* **293**, 259 (2010).
- W. F. McDonough, in *The Mantle and Core*, R. W. Carlson, Ed., vol. 2 of *Treatise on Geochemistry*, H. Holland, K. K. Turekian, Eds. (Elsevier-Pergamon, Oxford, 2003), pp. 547–568.
- D. Antonangeli *et al.*, *Earth Planet. Sci. Lett.* **295**, 292 (2010).
- J. Badro *et al.*, *Earth Planet. Sci. Lett.* **254**, 233 (2007).
- D. C. Rubie, C. K. Gessmann, D. J. Frost, *Nature* **429**, 58 (2004).
- K. J. Walsh, A. Morbidelli, S. N. Raymond, D. P. O'Brien, A. M. Mandell, *Nature* **475**, 206 (2011).

Acknowledgments: The research leading to these results has received funding from the European Research Council (ERC) under the European Community's Seventh Framework Programme (FP7/2007-2013)/ERC grant agreement 207467. This work was performed under the auspices of the Lawrence Livermore National Laboratory, U.S. Department of Energy, under contract DE-AC52 07NA27344 and was supported by the Office of Basic Energy Sciences, Geosciences Research Program (F.J.R.). The Focused Ion Beam (FIB) facility of the IMPMC is supported by Région Ile de France grant SESAME 2006 N°1-07-593/R, INSU-CNRS, Institut de Physique (INP) CNRS, University Pierre et Marie Curie–Paris 6, and French National Research Agency (ANR) grant ANR-07-BLAN-0124-01 (J.B.). We thank I. Esteve for assistance during sample preparation with the FIB, and G. Garbarino for assistance on the high-pressure beamline (ID27) of the European Synchrotron Radiation Facility.

Supplementary Materials

www.sciencemag.org/cgi/content/full/science.1227923/DC1
Materials and Methods
Supplementary Text
Figs. S1 and S2
Tables S1 to S5
References (34–50)

25 July 2012; accepted 20 December 2012
Published online 10 January 2013;
10.1126/science.1227923